

Template synthesized gold nanotube membranes for chemical separations and sensing

Marc Wirtz, Shufang Yu and Charles R. Martin*

Department of Chemistry and Center for Research at the Bio/Nano Interface, University of Florida, Gainesville, FL 32611, USA. E-mail: crmartin@chem.ufl.edu

Received 22nd February 2002, Accepted 26th March 2002
 First published as an Advance Article on the web 14th May 2002

We have developed a new class of synthetic membranes that consist of a porous polymeric support that contains an ensemble of gold nanotubes that span the thickness of the support membrane. The support is a commercially-available microporous polycarbonate filter with cylindrical nanoscopic pores. The gold nanotubes are prepared *via* electroless deposition of Au onto the pore walls; *i.e.*, the pores acts as templates for the nanotubes. We have shown that by controlling the Au deposition time, Au nanotubes that have effective inside diameters of molecular dimensions (< 1 nm) can be prepared. These membranes are a new class of molecular sieves and can be used to separate both small molecules and proteins on the basis of molecular size. In addition, the use of these membranes in new approaches to electrochemical sensing is reviewed here. In this case, a current is forced through the nanotubes, and analyte molecules present in a contacting solution phase modulate the value of this transmembrane current.

1. Introduction

We have been investigating a general method for preparing nanomaterials called template synthesis.^{1–3} This method entails synthesis or deposition of the desired material within the cylindrical and monodisperse pores of a nanopore membrane or other solid. We have used polycarbonate filters, prepared *via* the track-etch method,⁴ and nanopore aluminas, prepared electrochemically from Al foil,⁵ as our template materials. Cylindrical nanostructures with monodisperse diameters and lengths are obtained, and depending on the membrane and synthetic method used, these may be solid nanowires or hollow nanotubes. We, and others, have used this method to prepare nanowires and tubes composed of metals,^{5–15} polymers,^{16–19} semiconductors,^{20,21} carbons,^{22–24} and Li⁺ intercalation materi-

als.^{25–27} It is also possible to prepare composite nanostructures, both concentric tubular composites, where an outer tube of one material surrounds an inner tube of another,^{28,29} and segmented composite nanowires.³⁰

One of our earliest applications of the template method was to prepare ensembles of microscopic^{31,32} and nanoscopic^{33,34} electrodes. Such electrodes are prepared by depositing noble metals within the pores of the polycarbonate filtration membranes. Initially, we deposited the metal in the pores using electrochemical-plating methods,³¹ but we ultimately discovered that electroless plating allowed for more uniform metal deposition.³³ In the electroless method, metal deposition begins at the pore walls creating, at short deposition time, hollow metal nanotubes within the pores^{8–12,35,36} That is, the electroless plating method yields metal (typically gold) nanotube membranes, the subject of this review.

Coincidentally, there is also a long-standing interest in our research group in the area of membrane-based chemical separations.^{37–39} This interest led us to undertake a series of fundamental investigations of the transport properties of the gold nanotube membranes. We discovered that by controlling the deposition time, we could prepare Au nanotubes that had effective inside diameters of molecular dimensions (< 1 nm).⁹ This suggested that these membranes might be useful as molecular sieves. In addition, because these membranes are composed of an electronically conductive material, it occurred to us that excess charge could be applied to the tubes by electrochemical charging in an electrolyte solution. We reasoned that it might be possible to use this excess charge to regulate ion-transport across these membranes.^{8,35} Furthermore, because the tubes are composed of gold, it seemed possible that we could use well-known Au–thiol chemistry to change the chemical environment within the tubes, and *via* this route, introduce chemical transport selectivity into these membranes.^{10–12,36} Finally, we have shown that the Au nanotube membranes can be used in a new electrochemical sensing system that offers extraordinary sensitivity.^{40,41}

In this paper we review the concept of molecular sieving, as applied to small molecules and proteins. We further discuss the use of the Au nanotube membranes as chemical sensors. We begin by briefly reviewing some of the experimental details

Charles R. Martin is Professor of Chemistry and Director of the Center for Research at the Bio/Nano Interface at the University of Florida. His research interests lie at the interfaces between analytical chemistry, electrochemistry and materials science. Areas of special interest include nanomaterials and nanoporous membranes for chemical and bioseparations and analyses, molecular-recognition membranes, electrochemistry of nanoscopic electrodes and materials, and electrochemical energy storage and production. He received his B.S. degree at the Centre College of Kentucky. He did graduate work at the University of Arizona with Henry Freiser and postdoctoral work at the University of Texas with Allen Bard. He started his academic career at Texas A&M University in 1981, moved to Colorado State University in 1990, and then to the University of Florida in 1999.



such as membranes used, the electroless plating method, and the gas flux method used to determine nanotube inside diameter. We then discuss investigations of molecular-size-based transport selectivity. This is followed by a discussion of an extremely sensitive chemical sensing method utilizing the Au nanotube membranes.

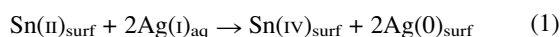
2. Membrane preparation and analysis

A. Template membranes and electroless plating

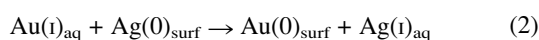
Commercially-available 'track-etched' polycarbonate filters are used as the templates to prepare the Au nanotubes. The track-etch process⁴ entails bombarding a solid material (in this case a ~10 μm-thick polycarbonate film) with a collimated beam of high-energy nuclear fission fragments to create parallel damage tracks in the film. The damage tracks are then etched into monodisperse cylindrical pores by exposing the film to a concentrated solution of aqueous base. The diameters of the pores are determined by the etch time and the etch-solution temperature. The density of pores is determined by exposure time to the fission-fragment beam. Membranes with pore diameters ranging from as small as 10 nm to as large as ~10 μm are available commercially.

The membranes used for these studies had nominal pore diameters of 30 nm and contained 6×10^8 pores per cm² of membrane surface area. The nominal pore diameter (supplied by the manufacturer) is obtained from scanning electron microscopic images of the film surface. Microscopic investigations of template-synthesized nanostructures prepared within the pores of such membranes have shown that the diameter of the pore in the center of the membrane is larger than the diameter at the membrane surface; *i.e.*, that cigar-shaped pores are obtained.^{14,17} It has been suggested that this pore geometry arises because the fission fragment that creates the damage track also generates secondary electrons, which contribute to the damage along the track.¹⁴ The number of secondary electrons generated at the faces of the membrane is less than in the central region of the membrane, and this is why 'bottleneck' pores are obtained.

The electroless plating method used to deposit the Au nanotubes within the pores of these membranes has been described previously.^{11,33} Briefly, the template membrane is first 'sensitized' by immersion into a SnCl₂ solution which results in deposition of Sn(II) onto all of the membrane's surfaces (pore walls and membrane faces). The sensitized membrane is then immersed into a AgNO₃ solution, and a surface redox reaction occurs (eqn. (1)) which yields nanoscopic metallic Ag particles on the membrane surfaces.



(The subscripts surf and aq denote species adsorbed to the membrane surfaces and species dissolved in solution, respectively.) The membrane is then immersed into a commercial gold plating solution and a second surface redox reaction occurs, to yield Au nanoparticles on the surfaces (eqn. (2)).



These surface-bound Au nanoparticles are good autocatalysts for the reduction of Au(I) to Au(0) using formaldehyde as the reducing agent. As a result, Au deposition begins at the pore walls, and Au tubes are obtained within the pores.^{8–12,35,36} In addition, the faces of the membrane become coated with thin Au films. These surface films do not, however, block the mouths of the nanotubes, and there are open nanoscopic channels running from one face of the membrane to the other. By controlling the electroless plating time, the inside diameter of these nanotubes can be controlled at will, down to molecular dimensions.

B. Estimation of the nanotube inside diameter

We use a gas-transport method to obtain an estimate of the inside diameter (id) of the template-synthesized Au nanotubes.¹¹ Briefly, the tube-containing membrane is placed in a gas-permeation cell, and the upper and lower half-cells are evacuated. The upper half-cell is then pressurized, typically to 20 psi with H₂, and the pressure–time transient associated with leakage of H₂ through the nanotubes is measured using a pressure transducer in the lower half-cell. The pressure–time transient is converted to gas flux (Q , mol s⁻¹) which is related to the radius of the nanotubes (r , cm) via^{11,42}

$$Q = 4/3(2\pi/MRT)^{1/2}(nr^3\Delta P/l) \quad (3)$$

where ΔP is the pressure difference across the membrane (dynes cm⁻²), M is the molecular weight of the gas, R is the gas constant (erg K⁻¹ mol⁻¹), n is the number of nanotubes in the membrane sample, l is the membrane thickness (cm) and T is the temperature (K).

In using eqn. (3) we assume: (i) that we know the number of nanotubes (n) in the membrane sample; (ii) that the nanotubes have a constant inside diameter down their entire length; and (iii) that the mechanism of gas transport through the membrane is Knudsen diffusion in the nanotubes. We have discussed the validity of each of these assumptions in detail in a recent review.⁴³

3. Molecular sieving and filtration in the Au nanotube membranes

Molecular sieving experiments were conducted using a simple U-tube permeation cell, where the membrane to be studied separates the 'feed' and 'permeate' half-cells. The feed half-cell is an aqueous solution containing the molecule or molecules whose transport properties are to be evaluated. The permeate half-cell initially contains only water or a salt solution. Passive diffusion drives the permeate molecule from the feed half-cell through the membrane and into the permeate half-cell. The time course of the transport process is followed by periodically assaying the permeate half-cell for the permeate molecule(s). The transport data are graphed as plots of moles of permeate molecule transported vs. permeation time.^{9–12} Straight-line plots are typically obtained, and the flux of the permeate molecule can be calculated from the slope. We will call such plots 'flux plots' in this review.

A. Molecular sieving in single-molecule permeation experiments

In these experiments, the flux plot for a particular molecule is determined with only that molecule present in the feed solution. The feed solution is then replaced with a solution of a second molecule and the flux plot for this molecule is obtained for the same membrane. A membrane-transport selectivity coefficient (α) can then be obtained by ratioing the fluxes for the two permeate molecules. Since molecular-sized based selectivity is of interest here, one of the permeate molecules used was large, the tris-bipyridal complex of Ru(II), Ru(bpy)₃²⁺, and the other was smaller, methyl viologen, MV²⁺ (Fig. 1).

The ratio of the diffusion coefficients for MV²⁺ and Ru(bpy)₃²⁺ in free aqueous solution is 1.5.^{40,43} For this reason, if a simple solution-like diffusion process were operative in the nanotubes, a selectivity coefficient of $\alpha = 1.5$ would be anticipated. In contrast, even for the largest id nanotubes investigated (5.5 nm), the selectivity coefficient was substantially greater, $\alpha = 50$ (Fig. 2A).⁹ These data show that size-based molecular sieving occurs in these large-id (>molecular dimensions) nanotubes.

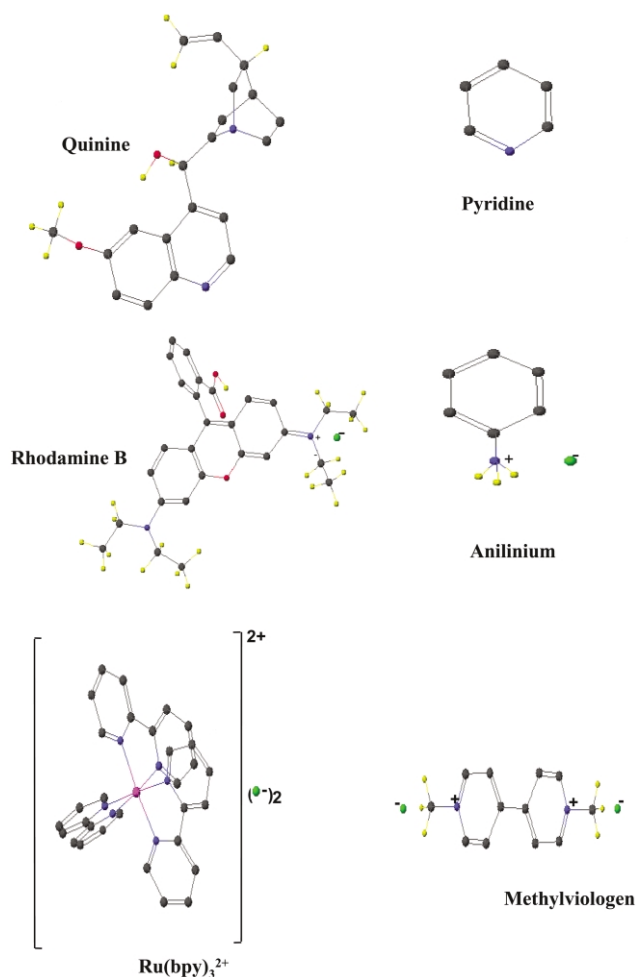


Fig. 1 Chemical structures and approximate relative sizes of the three 'big molecule/small molecule' pairs used in the molecular filtration experiments. Quinine, MV²⁺, and Ru(bpy)₃²⁺ were also used as analytes in the sensor work.

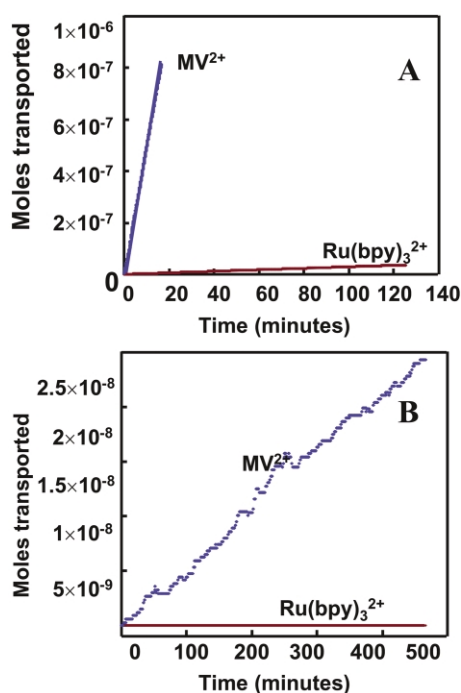


Fig. 2 Single-molecule permeation experiments showing moles of MV²⁺ and Ru(bpy)₃²⁺ transported versus time. Membranes contained nanotubes with ids of (A) 5.5 nm. (B) < 0.6 nm. Only MV²⁺ was transported through this membrane.

Molecular-sieving is a result of hindered diffusion of the molecules in the Au nanotubes.⁴⁴ The simplest way to understand hindered diffusion is to consider first the Stokes–Einstein equation that relates the diffusion coefficient (D_s) to the molecular radius (r_{mol}) for diffusion in free solution (eqn. (4))

$$D_s = kT/6\pi\eta r_m \quad (4)$$

where k is the Boltzmann constant, T is the Kelvin temperature, and η is the viscosity. The denominator $6\pi\eta r_m$ can be thought of as a molecular-friction coefficient that determines the resistance to diffusion in the solution. As would be expected, this molecular-friction term increases with increasing size of the molecule and increasing viscosity of the solution.

In the Au nanotube membranes, this molecular-friction coefficient is larger than in free solution because collisions with the nanotube wall increase the frictional drag on the molecule.⁴⁵ In addition, the rate of diffusive mass transport in the nanotube is decreased, relative to a contacting solution phase, because of steric reasons.⁴⁴ Consider a molecule of radius r_{mol} diffusing within a nanotube of comparable radius r_{tube} . The extent to which the diffusion coefficient for a molecule in the nanotube (D_{tube}) is decreased relative to its value in free solution (D_{sol}) is related to the parameter λ which is the ratio of the radius of the diffusing molecule to the radius of the nanotube⁴⁴

$$\lambda = r_{\text{mol}}/r_{\text{tube}} \quad (5)$$

A large number of theoretical expressions have been derived that predict how the ratio $D_{\text{tube}}/D_{\text{sol}}$ varies with λ .^{44–46} The extremes are easy to define; when $\lambda = 0$ ($r_{\text{mol}} \ll r_{\text{tube}}$) $D_{\text{tube}}/D_{\text{sol}} = 1$, and when λ approaches unity (tube and molecule are the same size) $D_{\text{tube}}/D_{\text{sol}}$ must approach zero. The Renkin equation (eqn. (6))

$$D_{\text{tube}}/D_{\text{sol}} = 1 - 2.104\lambda + 2.09\lambda^3 - 0.95\lambda^5 \quad (6)$$

is an often-used example of the relationship between $D_{\text{tube}}/D_{\text{sol}}$ and λ .⁴⁶ Plots of this equation and various other expressions for the relationship between $D_{\text{tube}}/D_{\text{sol}}$ and λ can be found in the literature.^{44–46}

Eqns. 5 and 6 show that for any nanotube id, diffusivity in the nanotube membrane will be lower for the larger Ru(bpy)₃²⁺ than for the smaller MV²⁺. This is reflected in the transport data (Fig. 2A) where the flux of the larger Ru(bpy)₃²⁺ is decreased more than the flux for the smaller MV²⁺. As a result $\alpha = 50$ is obtained.⁹ Eqns. 5 and 6 predict that as the nanotube id is made smaller, the α value should become even larger, which is also reflected in the transport data. Values for the 5.5 nm, 3.2 nm and 2.0 nm id nanotube membranes are $\alpha = 50, 88,$ and $172,$ respectively.⁹

B. Molecular filtration in two-molecule permeation experiments

The smallest id nanotube membrane investigated (id ~ 0.6 nm) provides a measurable flux for MV²⁺, but the larger Ru(bpy)₃²⁺ could not be detected in the permeate solution, even after a two week permeation experiment (Fig. 2B). These data suggest that clean separation (molecular filtration) of these two species should be possible with this nanotube membrane. This was proven by doing two-molecule permeation experiments, where both the larger and smaller molecules (Fig. 1) were present in the feed half-cell together. A simple U-tube cell was used, and the permeate solution was periodically assayed, using UV–vis absorption or fluorescence, for both molecules. For all three of the large-molecule/small-molecule pairs shown in Fig. 1, the small molecule could be easily detected in the permeate solution but the large molecule was undetectable⁹

These data show that within the limits of the measurement, the Au nanotube membrane can cleanly separate large mole-

cules from small molecules. However, one could argue that the large molecule is, indeed, present in the permeate solution but at a concentration just below the detection limit of the analytical method employed. This argument allows us to define a minimal transport selectivity coefficient (α_{\min}) for each small-molecule/large-molecule pair investigated, where α_{\min} is defined as the measured concentration of the small molecule in the permeate solution divided by the detection limit for the large molecule. The α_{\min} values obtained are extraordinary (Table 1). It is important to stress again that, in all three cases, the larger molecule was undetectable in the permeate solution.

4. Size-based separations of proteins

We have recently started investigating protein transport in the Au nanotube membranes.⁴⁷ In this case, the ability to tailor the chemistry of the Au nanotubes provides a route for suppressing protein adsorption and thus fouling, a vexing problem for ultrafiltration separations of proteins.^{48–53} In particular, there have been a number of investigations of protein transport in the track-etched polycarbonate membranes^{54–59} used as the templates to prepare the Au nanotubes, and protein adsorption has proven to be a problem in such studies.^{56–59} Protein adsorption to the Au nanotube membranes was suppressed by chemisorbing a thiol-terminated poly(ethylene glycol). It is well known that PEG-modified surfaces show decreased protein adsorption relative to the unmodified surface.^{60–65} The ability to precisely control the inside diameter (id) of the nanotubes (and to produce nanotubes with very monodisperse ids) is also advantageous in that this should allow for size-based separation of proteins of similar molecular weights. We describe results of preliminary investigations of protein separations in the Au nanotube membranes here. The effect of nanotube id on rate and selectivity of protein transport was investigated for three proteins: lysozyme (Lys), bovine serum albumin (BSA) and β -lactoglobulin (LGA).

The Au nanotube membranes were mounted between the two halves of a U-tube permeation cell as described above. Both single-protein and two-protein permeation experiments were done. Unless otherwise noted, this solution was forced through the membrane by applying 20 psi pressure to the feed half-cell. The permeate half-cell was initially empty. As solution was forced through the membrane, the permeate half-cell was periodically sampled and the concentration of the protein was determined *via* the UV absorbance at 280 nm. The two-protein permeation experiments were done in an analogous fashion except the feed solution was 0.025 mM in each protein. The concentration of each protein in the permeate half-cell was determined by sampling the permeate solution after ~ 1 mL was transported and doing HPLC analysis. In addition to these pressure-driven transport experiments, preliminary single-molecule permeation experiments were done in the absence of applied pressure. In this case, transport occurred by diffusion of the protein across the membrane into 5 mL of the buffer solution.

A. Single-protein permeation experiments

Fig. 3 shows results of single-protein (Lys) permeation experiments in the absence of applied pressure for id = 23 nm

Table 1 Minimal membrane-transport selectivity coefficients

Permeate pair	α_{\min}
Pyridine/quinine	15000
Anilinium/Rhodamine B	130000
MV ²⁺ /Ru(bpy) ₃ ²⁺	1500

Au nanotube membranes, with and without chemisorbed PEG-thiol. Without the PEG-thiol, transport stops after ~ 8 h, indicating rapid blockage of the nanotubes by adsorbed protein. In contrast, when the PEG-thiol is present, linear moles-transported vs. time data are obtained for up to 5 days. These data clearly show that protein adsorption is strongly suppressed by the chemisorbed PEG. This suppression of protein adsorption is also observed in the pressure-driven transport experiment, where protein flux is ~ 2 -orders of magnitude higher. Indeed, we have conducted such experiments for as long as 6 days with no evidence of protein adsorption. All of the remaining data presented in this section of the review are from membranes with chemisorbed PEG-thiol and where 20 psi pressure was used to drive the feed solution through the membrane.

Fig. 4 shows results of single-protein permeation experiments for Lys (upper line) and BSA (lower line) through a membrane with id = 40 nm gold nanotubes. The flux of Lys is 4-times higher than the flux of BSA. The Stokes radii for BSA and Lys are 3.6 nm and 2 nm, respectively;⁶⁶ hence, the Stokes–Einstein equation would predict that in free solution the diffusion coefficient for Lys would be only 1.8 times higher than that for BSA. That the ratio of the fluxes in the nanotube membrane (Fig. 4) is higher than this Stokes ratio is again indicative of hindered transport^{43,44} (see eqns. (5) and (6)) of the protein molecules in these nanoscopic tubes. Two-protein permeation experiments were used to explore this issue further.

B. Molecular filtration in two-protein permeation experiments

Fig. 5A shows HPLC data for the feed solution from a BSA/Lys two-protein permeation experiment. Fig. 5B shows HPLC data for an aliquot of the permeate solution after permeation through an id = 45 nm gold nanotube membrane. In analogy to the single-protein transport case (Fig. 4), the attenuation of the BSA peak, relative to the Lys peak, clearly shows the enhanced discrimination against the larger protein molecule. Fig. 5C shows analogous data after transport through an id = 30 nm nanotube membrane; now the BSA peak is barely discernable. BSA could not be detected in the permeate from an id = 20 nm nanotube membrane (Fig. 5D). This, of course, does not mean

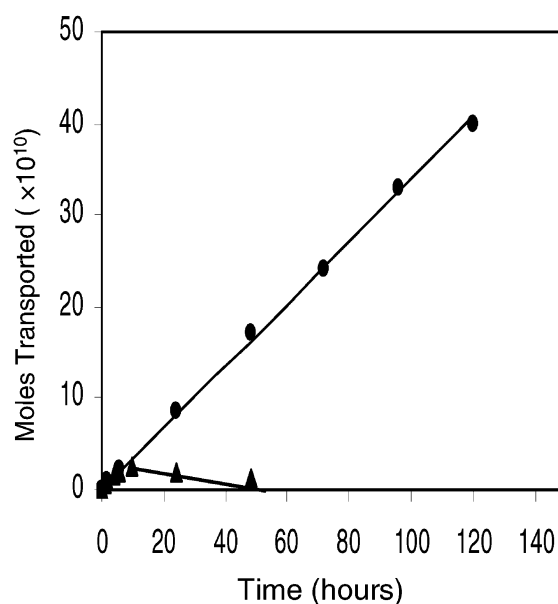


Fig. 3 Plots of moles transported vs. time for Lys diffusion (no applied pressure) across id = 23 nm Au nanotube membranes. Upper line, with chemisorbed PEG-thiol. Lower curve, no PEG thiol.

that there is no BSA present; it simply means that the concentration is below the detection limit of our analytical method, which for BSA is $\sim 0.2 \mu\text{M}$. In an attempt to obtain a discernable BSA signal in the permeate from the $\text{id} = 20 \text{ nm}$ nanotube membrane, we increased the permeation volume from

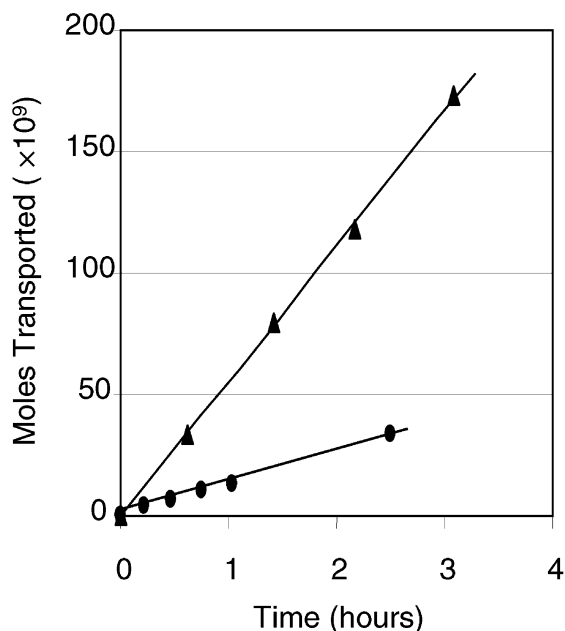


Fig. 4 Plots of moles transported vs. time for Lys (upper) and BSA (lower) across an $\text{id} = 40 \text{ nm}$ Au nanotube membrane. Single-protein permeation experiments.

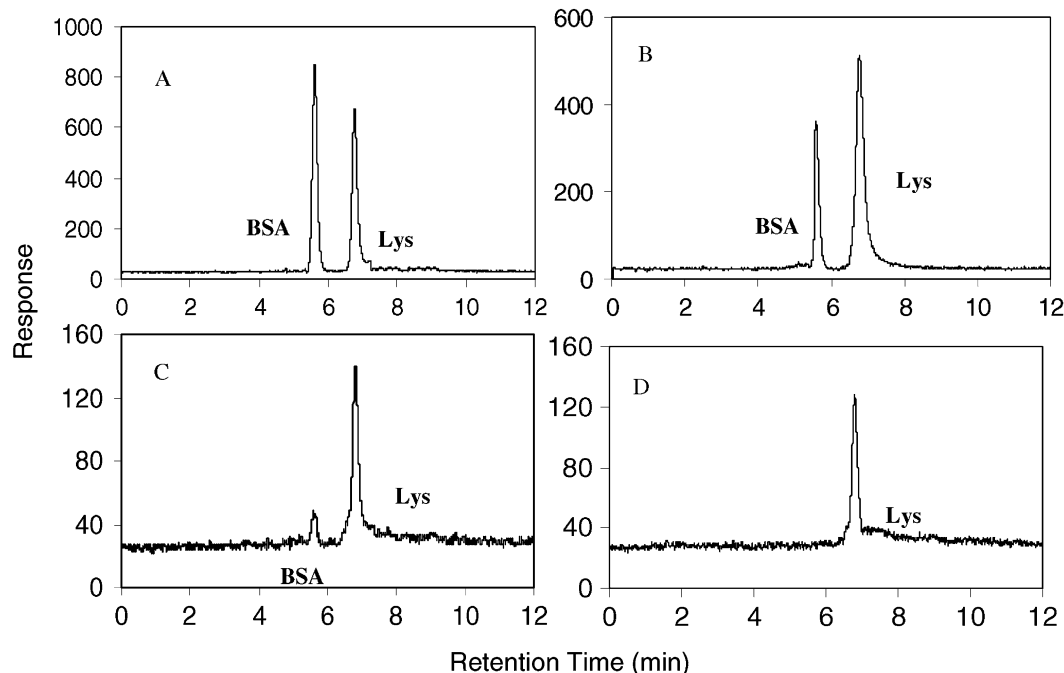


Fig. 5 HPLC data for two-protein (Lys/BSA) permeation experiments. (A) Feed solution. Permeate solutions after transport through $\text{id} = 45 \text{ nm}$ (B), 30 nm (C), and 20 nm (D) nanotube membranes.

Table 2 Concentrations of proteins in the permeate and transport selectivity coefficients for two-protein permeation experiments

Mixture of Lys and BSA				Mixture of LGA and BSA			
Id/nm	Conc. of Lys/ μM	Conc. of BSA/ μM	$\alpha_{\text{Lys/BSA}}$	Id/nm	Conc. of LGA/ μM	Conc. of BSA/ μM	$\alpha_{\text{LGA/BSA}}$
20	4.0	0	≥ 20	22	3.1	0	≥ 15
30	6.3	0.5	13	27	4.3	0.3	14
45	18.6	8.4	2.2	40	10.5	1.6	6.7

1 to 2 mL, but there was still no detectable BSA in the permeate.

The transport data in Fig. 5 can be quantified by defining a Lys vs. BSA selectivity coefficient, $\alpha_{\text{Lys/BSA}}$, which is the ratio of the concentration of Lys to the concentration of BSA in the permeate solution. Table 2 shows that $\alpha_{\text{Lys/BSA}}$ increases with decreasing nanotube diameter. These results are analogous to the small-molecule permeation in smaller-id Au nanotube membranes reviewed above. In the case of the $\text{id} = 20 \text{ nm}$ membrane, where BSA could not be detected, we report a minimal transport selectivity coefficient, defined as before⁹ as the detected concentration of the smaller protein (Lys) divided by the detection limit for the larger protein (BSA). As indicated in Table 2, the selectivity coefficient for the $\text{id} = 20 \text{ nm}$ nanotube membrane is at least 20. That this difference in selectivity is based primarily on the difference in size and not charge of the proteins is reinforced by the fact that at this pH value, BSA is negatively charged and Lys is positively charged.^{48,66} Furthermore, the PEG is electrically neutral so there should be no excess charge on the nanotubes.

Table 2 also shows that the increased selectivity for the membranes containing the smaller id nanotubes comes at a price, the flux of both proteins across the membrane decreases with decreasing nanotube diameter. Hence, as is typically observed in membrane-based separations processes, membranes that show higher selectivity also show decreased permeate throughput or productivity.⁶⁷ Fig. 6 shows analogous data for the separation of BSA from LGA and the corresponding selectivity coefficients are also tabulated in Table 2. Again, we see higher selectivity and lower productivity for the membranes containing the smaller id nanotubes.

These studies have shown that by controlling the ids of the nanotubes, Au nanotube membranes can show good selectivity

for separation of proteins on the basis of molecule size. In addition, by chemisorbing a PEG–thiol, the problem of membrane fouling by protein adsorption can be eliminated. Protein flux in these experiments was enhanced by applying a pressure difference across the membrane. We are currently investigating electrophoresis of proteins across such membranes. This not only provides an alternative method for enhancing flux but also adds the dimension of using protein charge as a way of further discriminating between proteins. Finally, while the Au nanotube membranes are good model systems for investigating how pore size and chemistry affect protein transport, the porosities of these membranes are too low for practical use in protein separations. We are currently investigating similar membranes with significantly higher porosities.

5. Chemical sensing with the Au nanotube membranes

In addition to the above possible applications in size-based separations, these Au nanotube membranes have been used as sensors for the determination of ultratrace concentrations of ions and molecules.^{40,41,68} In this case, the nanotube membrane was allowed to separate two salt solutions, a constant transmembrane potential was applied, and the resulting transmembrane current was measured. When an analyte of comparable dimensions to the inside diameter of the nanotubes was added to one of the salt solutions, a decrease in transmembrane current was observed. The magnitude of this drop in transmembrane current (Δi) is proportional to the analyte concentration.

A. Calibration curves and detection limits

As in the transport experiments, a U-tube cell was assembled with the nanotube membrane separating the two halves of the cell. The two half-cells were filled with the desired electrolyte and an electrode was placed into each half-cell. Three different sets of electrodes and electrolytes were used. The first set consisted of two Pt plate electrodes, and the electrolyte used in

both half-cells was 0.1 M KF. The second set consisted of two Ag/AgCl wires, and the electrolyte used in both half-cells was 0.1 M KCl. The third set consisted of two Ag/AgI wires immersed in 0.1 M KI.

As noted above, the experimental protocol used with these cells was to immerse the electrodes into the appropriate electrolyte and apply a constant potential between the electrodes. The resulting transmembrane current was measured and recorded on an $X-t$ recorder. After obtaining this baseline current, the anode half-cell was spiked with a known quantity of the desired analyte (Fig. 1). This resulted in a change in the transmembrane current, Δi (Fig. 7). A potentiostat was used to apply the potential between the electrodes and measure the transmembrane current. The transmembrane potential used was of the order of 0.5 V.^{40,68}

Plots of $\log \Delta i$ vs. $\log[\text{analyte}]$ for the analytes $\text{Ru}(\text{bpy})_3^{2+}$, MV^{2+} and quinine (Fig. 1) were obtained using Ag/AgCl electrodes and 0.1 M KCl as the electrolyte in both half-cells (Fig. 8). For these experiments, a membrane with 2.8 nm id Au nanotubes was used. A log–log format is used for these “calibration curves” because of the large dynamic range (spanning as much as five orders of magnitude in analyte concentration) obtained with this cell. Analogous calibration curves were obtained for the other electrode/electrolyte systems investigated. The detection limits⁴⁰ obtained are shown in Table 3. For the divalent cationic electrolytes, the detection limits were lowest (best) in the Ag/AgI/KI cell and worst in the Pt/KF cell. The detection limit for quinine was the same in both the Ag/AgI/KI and Ag/AgCl/KCl cells. In general, the detection limit decreases as the size of the analyte molecule increases (see Fig. 1). Finally, the detection limits obtained (down to 10^{-11} M) are extraordinary and compete with even the most sensitive of modern analytical methods.

The majority of the quinine in both the KCl and KI solutions is present as the monoprotonated (monocationic) form. Perhaps the reason the detection limits for $\text{Ru}(\text{bpy})_3^{2+}$ and MV^{2+} are lower in the Ag/AgI/KI cell while the detection limit for quinine is the same in both this cell and the Ag/AgCl/KCl cell has to do with the difference in charge of these analytes (predominately monocationic vs. dicationic). To explore this point, the detection limits for a neutral analyte, 2-naphthol, were obtained in both the Ag/AgI/KI and Ag/AgCl/KCl cells. Like quinine,

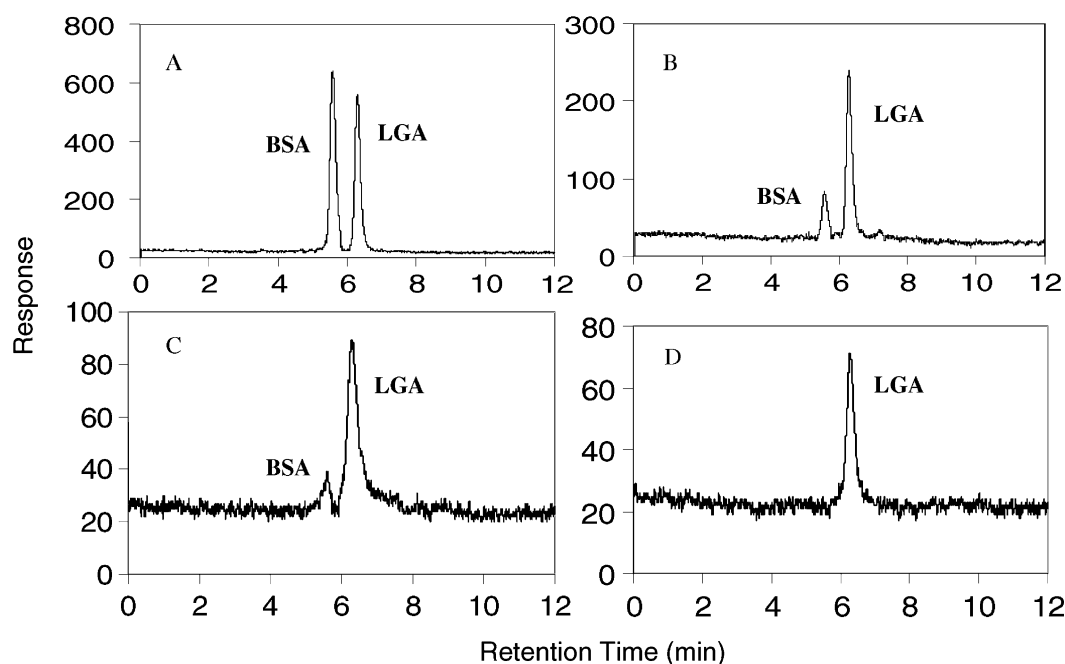


Fig. 6 HPLC data for two-protein (LGA/BSA) permeation experiments. (A) Feed solution. Permeate solutions after transport through id = 40 nm (B), 27 nm (C), and 22 nm (D) nanotube membranes.

the detection limit for this neutral analyte was the same in both cells (10^{-6} M, Table 3).

In the membrane transport studies it was shown that $\text{Ru}(\text{bpy})_3^{2+}$ and MV^{2+} come across such membranes as the ion multiples $\text{Ru}(\text{bpy})_3^{2+}(\text{X}^-)_2$ and $\text{MV}^{2+}(\text{X}^-)_2$ ($\text{X}^- = \text{anion}$).⁹ In the KI cell, the ion multiple contains two larger (relative to

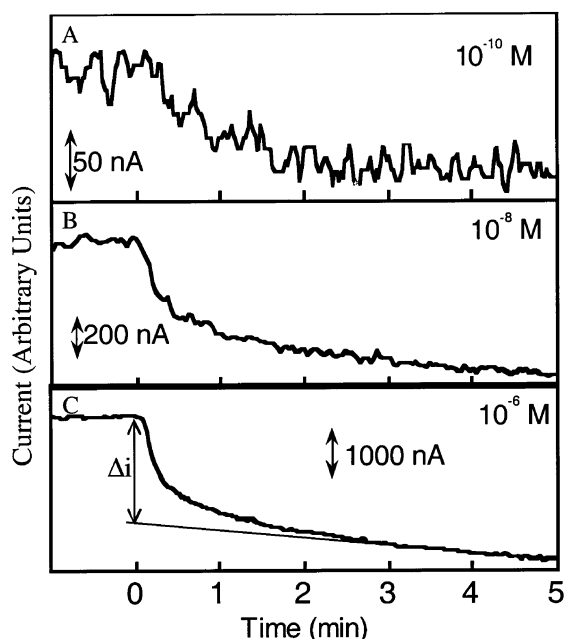


Fig. 7 Nanotube membrane sensor current–time transients associated with spiking the anode half cell with the indicated concentrations of $\text{Ru}(\text{bpy})_3^{2+}$. Tube id = 2.8 nm; Ag/AgCl/KCl cell Δi determined as shown in C.

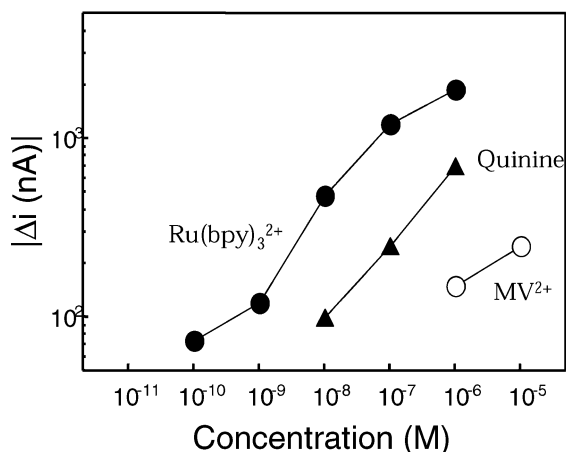


Fig. 8 Calibration curves for the indicated analytes. Membrane and cell as per Fig. 7.

Table 3 Detection limits obtained using the constant–potential method. The membrane contained ~ 2.8 nm diameter tubules

Cell	Analyte	Detection limit/M
Pt/KF	$\text{Ru}(\text{bpy})_3^{2+}$	10^{-9}
Ag/AgCl/KCl	$\text{Ru}(\text{bpy})_3^{2+}$	10^{-10}
	Quinine	10^{-8}
	MV^{2+}	10^{-6}
	2-Naphthol	10^{-6}
Ag/AgIKI	$\text{Ru}(\text{bpy})_3^{2+}$	10^{-11}
	Quinine	10^{-8}
	MV^{2+}	10^{-7}
	2-Naphthol	10^{-6}

chloride) iodide anions. Perhaps the larger size of the iodide ion multiple accounts for the lower detection limit in the KI-containing cell. If this is true then the difference between the quinine cation paired with one I^- vs. this cation paired with one Cl^- is not great enough to cause the detection limit for this predominately monovalent analyte to be significantly different in the Ag/AgI/KI vs. the Ag/AgCl/KCl cells (Table 3).

The final variable to be investigated is the effect of nanotube inside diameter on detection limit. To explore this parameter, membranes with nanotube inside diameters of approximately of 3.8, 2.8, 2.2, 1.8, and 1.4 nm were prepared and used in the Ag/AgI/KI cell.⁴⁰ Calibration curves for the analytes $\text{Ru}(\text{bpy})_3^{2+}$, MV^{2+} and quinine were generated as before, and detection limits were obtained from these calibration curves. Fig. 9 shows plots of detection limits for these three different analytes vs. the nanotube inside diameter in the membrane used. A minimum in this plot is observed for each of the three analytes.

The nanotube membrane that produces the minimum (best) detection limit depends on the size of the analyte. These molecules decrease in size in the order $\text{Ru}(\text{bpy})_3^{2+} > \text{quinine} > \text{MV}^{2+}$. The nanotube membrane that yields the lowest detection limit follows this size order; that is, the nanotube diameters that produce the lowest detection limit for $\text{Ru}(\text{bpy})_3^{2+}$, quinine, and MV^{2+} are 2.8 nm, 2.2 nm, and 1.8 nm, respectively. For the roughly spherical analytes, the optimal tube diameter is a little over twice the diameter of the molecule.

B. Molecular size based selectivity

The data presented above show a strong correlation between detection limit and the relative sizes of the nanotube and the analyte molecule (Fig. 8). This indicates that this device should show molecular-size-based selectivity. This is not surprising given the transport studies discussed previously. To explore size-based selectivity, a series of solutions were prepared containing decreasing concentrations of the analyte species, but containing a constant (higher) concentration of an interfering species. The interfering species was smaller than the analyte species. The response of the nanotube membrane (nanotube diameter = 2.8 nm) to these solutions was then measured starting from lowest to highest concentration of the analyte species.

The small pyridine molecule was used as the first interfering species. When present at a concentration of 10^{-4} M, pyridine offered very little interference for any of the analytes $\text{Ru}(\text{bpy})_3^{2+}$, MV^{2+} or quinine. The detection limits in the presence of 10^{-4} M pyridine were 10^{-10} M for $\text{Ru}(\text{bpy})_3^{2+}$, 10^{-6} M for MV^{2+} and 10^{-7} M for quinine, within an order of

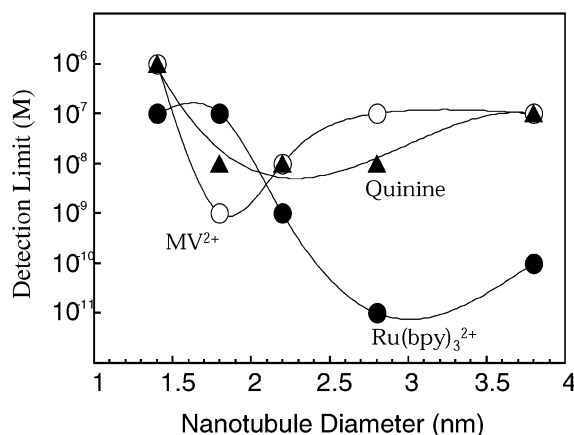


Fig. 9 Detection limits for MV^{2+} , quinine, and $\text{Ru}(\text{bpy})_3^{2+}$ vs. id of the nanotubes used in the sensor.

magnitude of the detection limit with no added interfering species (Table 3). Put another way, this nanotube membrane sensor can detect 10^{-10} M $\text{Ru}(\text{bpy})_3^{2+}$ in the presence of six orders of magnitude higher pyridine concentration. A second set of experiments was done using the larger MV^{2+} as the interfering species. Now at low concentrations of analyte, there is a region where the device produces a constant response due to the constant concentration (10^{-4} M) of this interfering species; *i.e.*, the much higher concentration of the MV^{2+} swamps the response of the device. However, as the concentration of $\text{Ru}(\text{bpy})_3^{2+}$ increases, there is a concentration range where the device responds to this analyte species without interference from the MV^{2+} . This concentration range begins at concentrations of $\text{Ru}(\text{bpy})_3^{2+}$ above 10^{-8} M. That is, the size-based selectivity is such that the larger analyte species, $\text{Ru}(\text{bpy})_3^{2+}$, can be detected down to 10^{-8} M in the presence of four orders of magnitude higher concentration of the smaller interfering species, MV^{2+} .

These data can be quantified by defining the selectivity coefficient $K_{\text{bpy}/\text{MV}}$ as the slope of the calibration curve for the analyte, $\text{Ru}(\text{bpy})_3^{2+}$, divided by the slope for the interfering species, MV^{2+} . This analysis is somewhat problematic because the calibration curves are nonlinear and because the device is not very sensitive to MV^{2+} .⁴⁰ However, taking the data from the central part of the $\text{Ru}(\text{bpy})_3^{2+}$ calibration curve gives a slope of $\sim 400 \text{ A M}^{-1}$; dividing by the slope for the MV^{2+} data gives $K_{\text{bpy}/\text{MV}} = 4,000$. These experiments show that, in agreement with the transport studies, the nanotube membrane-based sensor can show excellent size-based selectivity.

Conclusion

In this review, we have discussed the use of Au nanotube membranes to separate molecules on the basis of size. We have shown here that these membranes can act as extraordinary molecular sieves. In addition, this molecular sieving has been extended to biological molecules. We have shown that this allows for controlling protein-transport selectivity in these membranes. Furthermore, we have described a new and highly-sensitive method of electroanalysis based on these membranes.

Besides showing size-based selectivity, previous studies have demonstrated that these Au nanotube membranes can show ionic charge-based transport selectivity and that the membranes can be electrochemically switched between anion transporting and cation transporting states.⁷² Hence, these membranes can be viewed as universal ion-exchangers. Furthermore, chemical transport selectivity can be introduced into these membranes by chemisorbing thiols to the inside tube walls.^{10,11} In this case, the chemisorbed thiol changes the chemical environment within the nanotubes and this, in turn, changes the transport properties of the membrane. For example, membranes modified with hydrophobic thiols selectively transport hydrophobic molecules.¹¹ Hence, these nanotube membranes can utilize all of the selectivity paradigms (sterics, electrostatics, and chemical interactions) that Mother Nature uses in the design of her exquisitely selective molecular-recognition schemes. Mother Nature also makes nanotubes (*e.g.*, protein⁶⁹ and ion channels^{70,71}), and again she uses size, charge and chemical interactions to determine what chemical species have access to these channels. The Au nanotube membranes can also be viewed as model systems for these naturally-occurring nanotubes. Furthermore, the Au nanotubes can perhaps be used to mimic transport in the natural channel systems. Such research at the bio/nano interface is of great current interest in our group.

Acknowledgements

Aspects of this work were funded by the National Science Foundation, the Office of Naval Research and the Department of Energy.

References

- 1 C. R. Martin, *Science*, 1994, **266**, 1961–1966.
- 2 J. C. Hulteen and C. R. Martin, *J. Mater. Chem.*, 1997, **7**, 1075–1087.
- 3 C. R. Martin and D. T. Mitchell, *Anal. Chem.*, 1998, **70**, 322A–327A.
- 4 R. L. Fleischer, P. B. Price and R. M. Walker, *Nuclear Tracks in Solids*, University of California Press, Berkeley, CA, 1975.
- 5 G. L. Hornyak, C. J. Patrissi and C. R. Martin, *J. Phys. Chem B*, 1997, **101**, 1548–1555.
- 6 G. E. Possin, *Rev. Sci. Instrum.*, 1970, **41**, 772.
- 7 W. D. Williams and N. Giordano, *Rev. Sci. Instrum.*, 1984, **55**, 410.
- 8 M. Nishizawa, V. P. Menon and C. R. Martin, *Science*, 1995, **268**, 700–702.
- 9 K. B. Jirage, J. C. Hulteen and C. R. Martin, *Science*, 1997, **278**, 655–658.
- 10 J. C. Hulteen, K. B. Jirage and C. R. Martin, *J. Am. Chem. Soc.*, 1998, **120**, 6603–6604.
- 11 K. B. Jirage, J. C. Hulteen and C. R. Martin, *Anal. Chem.*, 1999, **71**, 4913–4918.
- 12 Z. Hou, N. L. Abbott and P. Stroeve, *Langmuir*, 2000, **16**, 2401–2404.
- 13 G. Tourillon, L. Pontonnier, J. P. Levy and V. Langlais, *Electrochem. Solid-State Lett.*, 2000, **3**, 20–23.
- 14 C. Schonenberger, B. M. I. van der Zande, L. G. J. Fokkink, M. Henry, C. Schmid, M. Kruger, A. Bachtold, R. Huber, H. Birk and U. Staufer, *J. Phys. Chem. B*, 1997, **101**, 5497–5505.
- 15 C. K. Preston and M. J. Moskovits, *J. Phys. Chem.*, 1993, **97**, 8405.
- 16 C. R. Martin, in *Handbook of Conducting Polymers*, ed. J. R. Reynolds, T. Skotheim and R. Elsebaumer, Marcel Dekker, New York, 2nd edn., 1997, ch. 16, pp. 409–421.
- 17 J. Duchet, R. Legras and S. Demoustier-Champagne, *Synth. Met.*, 1998, **98**, 113–122.
- 18 S. Demoustier-Champagne and P.-Y. Stavaux, *Chem. Mater.*, 1999, **11**, 829–834.
- 19 S. Sukeerthi and Q. Contractor, *Anal. Chem.*, 1999, **71**, 2231–2236.
- 20 B. B. Lakshmi, C. J. Patrissi and C. R. Martin, *Chem. Mater.*, 1997, **9**, 2544–2550.
- 21 B. B. Lakshmi, P. K. Dorhout and C. R. Martin, *Chem. Mater.*, 1997, **9**, 857–862.
- 22 G. Che, B. B. Lakshmi, C. R. Martin and E. R. Fisher, *Langmuir*, 1999, **15**, 750–758.
- 23 G. Che, E. R. Fisher and C. R. Martin, *Nature*, 1998, **393**, 346–349.
- 24 T. Kyotani, L. F. Tsai and A. Tomita, *Chem. Commun.*, 1997, 701.
- 25 C. J. Patrissi and C. R. Martin, *J. Electrochem. Soc.*, 1999, **146**, 3176–3180.
- 26 N. Li, C. J. Patrissi and C. R. Martin, *J. Electrochem. Soc.*, 2000, **147**, 2044–2049.
- 27 G. Che, K. B. Jirage, E. R. Fisher, C. R. Martin and H. Yoneyama, *J. Electrochem. Soc.*, 1997, **144**, 4296–4302.
- 28 V. M. Cepak, J. C. Hulteen, G. Che, K. B. Jirage, B. B. Lakshmi, E. R. Fisher and C. R. Martin, *J. Mater. Res.*, 1998, **13**, 3070–3080.
- 29 V. M. Cepak, J. C. Hulteen, G. Che, K. B. Jirage, B. B. Lakshmi, E. R. Fisher and C. R. Martin, *Chem. Mater.*, 1997, **9**, 1065–1067.
- 30 B. R. Martin, D. J. Dermody, B. D. Reiss, M. Fang, L. A. Lyon, M. J. Natan and T. E. Mallouk, *Adv. Mater.*, 1999, **11**, 1021–1025.
- 31 R. M. Penner and C. R. Martin, *Anal. Chem.*, 1987, **59**, 2625–2630.
- 32 I. F. Cheng and C. R. Martin, *Anal. Chem.*, 1988, **60**, 2163–2165.
- 33 V. P. Menon and C. R. Martin, *Anal. Chem.*, 1995, **67**, 1920–1928.
- 34 J. C. Hulteen, V. P. Menon and C. R. Martin, *J. Chem. Soc., Faraday Trans. 1*, 1996, **92**, 4029–4032.
- 35 M. S. Kang and C. R. Martin, *Langmuir*, 2001, **17**, 2753–2759.
- 36 S. B. Lee and C. R. Martin, *Anal. Chem.*, 2001, **73**, 768–775.
- 37 R. V. Parthasarathy, V. P. Menon and C. R. Martin, *Chem. Mater.*, 1997, **9**, 560–566.
- 38 W.-J. Chen and C. R. Martin, *J. Membr. Sci.*, 1995, **104**, 101–108.
- 39 C. Liu and C. R. Martin, *Nature*, 1991, **352**, 50–52.

- 40 Y. Kobayashi and C. R. Martin, *Anal. Chem.*, 1999, **71**, 3665–3672.
- 41 Y. Kobayashi and C. R. Martin, *J. Electroanal. Chem.*, 1997, **431**, 29–33.
- 42 W. J. Petzny and J. A. Quinn, *Science*, 1969, **166**, 751.
- 43 C. R. Martin, M. Nishizawa, K. B. Jirage and M. S. Kang, *J. Phys. Chem. B*, 2001, **105**, 1925–1934.
- 44 V. M. Deen, *AIChE J.*, 1987, **33**, 1409–1425.
- 45 I. A. Kathawalla, J. L. Anderson and J. S. Lindsey, *Macromolecules*, 1989, **22**, 1215–1219.
- 46 J. M. Nitsche and G. Balgi, *Ind. Eng. Chem. Res.*, 1994, **33**, 2242–2247.
- 47 S. Yu, S. B. Lee, M. Kang and C. R. Martin, *Nanoletters*, 2001, **1**(9), 495–498.
- 48 J. A. Howell, D. Wu and R. W. Field, *J. Membr. Sci.*, 1999, **152**, 117–127.
- 49 R. van Reis, J. M. Brake, J. Charkoudian, D. B. Burns and A. L. Zydney, *J. Membr. Sci.*, 1999, **159**, 133–142.
- 50 L. J. Zeman and A. L. Zydney, *Microfiltration and Ultrafiltration Principles and Applications*, Marcel Dekker, New York, 1996.
- 51 Q. Y. Li, Z. F. Cui and D. S. Pepper, *J. Membr. Sci.*, 1997, **136**, 181–190.
- 52 D. A. Musale and S. S. Kulkarni, *J. Membr. Sci.*, 1997, **136**, 13–23.
- 53 K. L. Jones and C. R. O'Melia, *J. Membr. Sci.*, 2000, **165**, 31–46.
- 54 A. K. Ho, J. M. Perera, D. E. Dunstan, G. W. Stevens and M. Nyström, *AIChE J.*, 1999, **45**, 1434–1450.
- 55 A. J. O'Connor, H. R. C. Pratt and G. W. Stevens, *Chem. Eng. Sci.*, 1996, **51**, 3459–3477.
- 56 C. Güell and R. H. Davis, *J. Membr. Sci.*, 1996, **119**, 269–284.
- 57 J. Mueller and R. H. Davis, *J. Membr. Sci.*, 1996, **116**, 47–60.
- 58 K. J. Kim, A. G. Fane, M. Nyström and A. Pihlajamaki, *J. Membr. Sci.*, 1997, **134**, 199–208.
- 59 C. Ho and A. L. Zydney, *J. Membr. Sci.*, 1999, **155**, 261–275.
- 60 H. B. Lu, C. T. Campbell and D. G. Castner, *Langmuir*, 2000, **16**, 1711–1718.
- 61 J. M. Harris, *Poly(ethylene glycol) Chemistry: Biotechnical and Biomedical Applications*, Plenum, New York, 1992.
- 62 M. Malmsten and J. M. Van Alstine, *J. Colloid Interface Sci.*, 1996, **177**, 502–512.
- 63 K. Emoto, J. M. Van Alstine and J. M. Harris, *Langmuir*, 1998, **14**, 2722–2729.
- 64 K. L. Prime and G. M. Whitesides, *Science*, 1991, **252**, 1164–1167.
- 65 P. Harber, M. Grunze, R. Dahint, G. M. Whitesides and P. E. Laibinis, *J. Phys. Chem. B*, 1998, **102**, 426–436.
- 66 S. R. Bellara, Z. Cui and D. S. Pepper, *Biotechnol. Prog.*, 1997, **13**, 869–872.
- 67 B. D. Freeman, *Macromolecules*, 1999, **32**, 375–380.
- 68 H. Bayley and C. R. Martin, *Chem. Rev.*, 2000, **100**, 2575–2594.
- 69 H. Bayley, *Sci. Am.*, 1997, 62.
- 70 D. Voet and J. G. Voet, *Biochemistry*, Wiley, New York, 2nd edn., 1995, pp. 1297.
- 71 H. Bayley and C. R. Martin, *Chem. Rev.*, 2000, **100**, 2575–2594.
- 72 M. Nishizawa, V. P. Menon and C. R. Martin, *Science*, 1995, **268**, 700–702.